Ocean Sci., 15, 527–541, 2019
https://doi.org/10.5194/os-15-527-2019

Ocean Science Open Access EGU

Long-term evolution of Caspian Sea thermohaline properties reconstructed in an eddy-resolving ocean general circulation model

Gleb S. Dyakonov[1,2] **and Rashit A. Ibrayev**[1,2,3]

[1]Northern Water Problems Institute, Russian Academy of Sciences, Petrozavodsk, Russia
[2]Shirshov Institute of Oceanology, Russian Academy of Sciences, Moscow, Russia
[3]Marchuk Institute of Numerical Mathematics, Russian Academy of Sciences, Moscow, Russia

Correspondence: Gleb S. Dyakonov (gleb.gosm@gmail.com)

Received: 31 October 2018 – Discussion started: 9 November 2018
Revised: 12 April 2019 – Accepted: 24 April 2019 – Published: 16 May 2019

Abstract. Decadal variability in Caspian Sea thermohaline properties is investigated using a high-resolution ocean general circulation model including sea ice thermodynamics and air–sea interaction forced by prescribed realistic atmospheric conditions and riverine runoff. The model describes synoptic, seasonal and climatic variations of sea thermohaline structure, water balance, and sea level. A reconstruction experiment was conducted for the period of 1961–2001, covering a major regime shift in the global climate during 1976–1978, which allowed for an investigation of the Caspian Sea response to such significant episodes of climate variability. The model reproduced sea level evolution reasonably well despite the fact that many factors (such as possible seabed changes and insufficiently explored underground water infiltration) were not taken into account in the numerical reconstruction. This supports the hypothesis relating rapid Caspian Sea level rise in 1978–1995 with global climate change, which caused variation in local atmospheric conditions and riverine discharge reflected in the external forcing data used, as is shown in the paper. Other effects of the climatic shift are investigated, including a decrease in salinity in the active layer, strengthening of its stratification and corresponding diminishing of convection. It is also demonstrated that water exchange between the three Caspian basins (northern, middle and southern) plays a crucial role in the formation of their thermohaline regime. The reconstructed long-term trends in seawater salinity (general downtrend after 1978), temperature (overall increase) and density (general downtrend) are studied, including an assessment of the influence of main surface circulation patterns and model error accumulation.

1 Introduction

The Caspian Sea is the largest enclosed water body on earth with a surface area of more than 370 000 km^2 and a catchment area almost 10 times greater. Yet it is highly sensitive to variations in the global and regional climate systems as well as economic activities that include major schemes of river regulation. This is vividly reflected in the evolution of the Caspian Sea level, which is subject to large fluctuations on seasonal and decadal timescales. The water balance of the isolated sea varies significantly due to the seasonal character of the riverine discharge, accounting for sea level oscillations with an amplitude of 20–40 cm. Long-term fluctuations of the level are even larger: in the second half of the 20th century they amounted to 2.5 m.

Prediction of the long-term impacts of climate change and man-made activities on the Caspian represents a great scientific challenge important for fisheries, coastal development and other industries of the region. Ocean general circulation models (OGCMs) have greatly advanced our understanding of the Caspian Sea circulation patterns, particularly its seasonal variability (Arpe et al., 1999; Ibrayev, 2008; Kara et al., 2010; Ibrayev et al., 2010; Gunduz and Özsoy, 2014; Diansky et al., 2016). The increasing production of global atmospheric reanalysis datasets and their availability over several decades have made possible retrospective studies of the long-term evolution of the marine environment based on numerical reconstruction of its response to external forcing, as will be done in the present paper. This approach was applied in our previous work (Dyakonov and Ibrayev, 2018) with emphasis on the long-term variability of the Caspian Sea water balance and its sensitivity to external factors. Now we

use the same model to study the evolution of thermohaline properties (temperature, salinity and density) of the Caspian Sea in 1961–2001. The period is particularly interesting, as it covers one of the most notable events of global climate change – the climate shift of 1976–1978, also referred to as the Great Pacific Climate Shift, widely discussed in the literature (Miller et al., 1994; Wooster and Zhang, 2004; Powell and Xu, 2011). The shift was associated with a change in major climatic indicators such as the North Atlantic Oscillation, with significantly increased cyclonic activity and air humidity in Europe consequently leading to a sharp rise in the Caspian Sea level and changes in its stratification. The weakened ventilation of the deep sea, in turn, has led to degradation of the ecological situation in the sea (Tuzhilkin et al., 2011).

In the present paper we analyze the long-term evolution of the Caspian Sea water parameters obtained in a numerical reconstruction experiment, which is described in Sect. 2. In order to better understand model results, the evolution of the prescribed atmospheric and riverine forcing is briefly considered in Sect. 3. In Sect. 4 we discuss main patterns of surface circulation, which will help explain further results. Then we proceed with model validation based on a comparison of the obtained evolution of several in situ parameters with observations (Sect. 5). Finally, in Sect. 6 we analyze the long-term variability of thermohaline properties of the sea and its response to climatic variations. The Caspian Sea comprises three basins, partly separated by peninsulas extending into the sea interior: northern, middle and southern (respectively referred to as NorthCS, MidCS and SouthCS). Due to great differences between the basins in terms of bottom relief, nonuniform distribution of river runoff and large sea extent in the latitude direction, the thermohaline circulation of each basin is distinctively different from the others. Therefore, the analyzed properties of water masses have been averaged over a certain horizon for every Caspian basin separately. Averaging in the horizontal plane simplifies the analysis but conceals many subbasin-scale features of the fields, which must be kept in mind. In the following figures vertical dashed lines mark instances in which climatic shifts occur.

2 Experiment setup

2.1 Model description

In Ibrayev (2001) and Ibrayev et al. (2001, 2010) a three-dimensional primitive equation numerical model MESH (Model for Enclosed Sea Hydrodynamics) was presented, which was developed to study Caspian Sea seasonal variability. The model successfully coped with this task and was used as the basis for the present research. However, an investigation of the Caspian Sea circulation on a decadal timescale imposes additional requirements on the model, and therefore it has been considerably redesigned. The geopotential vertical coordinate (z coordinate), which was used in MESH, was replaced by a hybrid system with a terrain-following sigma coordinate in the upper 30 m of the sea covering shallow regions and a z coordinate below 30 m of depth. The long-term fluctuations of the Caspian Sea surface height (CSSH) are greater than the seasonal by an order of magnitude and could cause numerical instabilities and errors in a z coordinate model. The use of a sigma coordinate ensures model stability during CSSH lows and allows for much better resolution of the surface boundary layer structure and diurnal air–sea interaction cycle during CSSH highs. A sigma coordinate grid also provides an accurate representation of the northern Caspian shelf bathymetry with increasingly flat slope (see Fig. 1). This is necessary to reconstruct the evolution of the sea surface area, which is essential for the evolution of air–sea fluxes in an environment of coastal flatlands subject to large CSSH fluctuations. Additionally, the model has been equipped with a flooding–drying algorithm, enabling it to describe shoreline variations related to mean sea level change and wind surges. A more detailed description of the model used in this work is presented in Ibrayev and Dyakonov (2016) and Dyakonov and Ibrayev (2016, 2018). Here we will note only the main points.

We use the Caspian Sea bathymetry based on the ETOPO1 dataset (Amante and Eakins, 2009), while particular attention has been paid to correctly interpolating the data onto the model grid and to preserving fine details such as islands and the shoreline. The Kara-Bogaz-Gol Bay was erased from the relief, as its connection to the sea is unilateral, and the corresponding boundary condition was set to account for the outflow of seawater into the bay. The resulting bathymetry is presented in Fig. 1. The model has a resolution of ~ 4.3 km in the horizontal plane, which is relatively high, as the Rossby baroclinic deformation radius is 17–22 km in deepwater areas of the Caspian (Arkhipkin et al., 1992). The eddy-resolving ability of the model is important to adequately simulate heat and salt transfer in the sea interior and obtain a correct circulation pattern. To ensure model stability without excessively damping the physical mode of its solution a parameterization of lateral viscosity has been implemented based on a bi-harmonic operator with Smagorinsky coefficient $C = 3$ as discussed in Griffies and Hallberg (2000). Lateral diffusivity is parameterized with a simple Laplacian scheme with constant coefficient $A_h = 1$. Heat and salt advection is approximated using a total variation diminishing scheme from Sweby (1984), which acts as a second-order scheme in most cases, except high-gradient frontal zones. In the vertical a grid is set with rather fine resolution varying from 2 m in the upper sea layer to 30 m in deep waters. This minimizes numerical errors in advection terms and prevents excessive accumulation of the errors in the long term. Vertical viscosity and diffusivity are parameterized via a scheme based on the Richardson number (Munk and Anderson, 1948) with variable coefficients: $K_m = (10^{-5}–10^{-3})\,\mathrm{m^2\,s^{-1}}$ for viscosity and $K_h = (10^{-7}–$

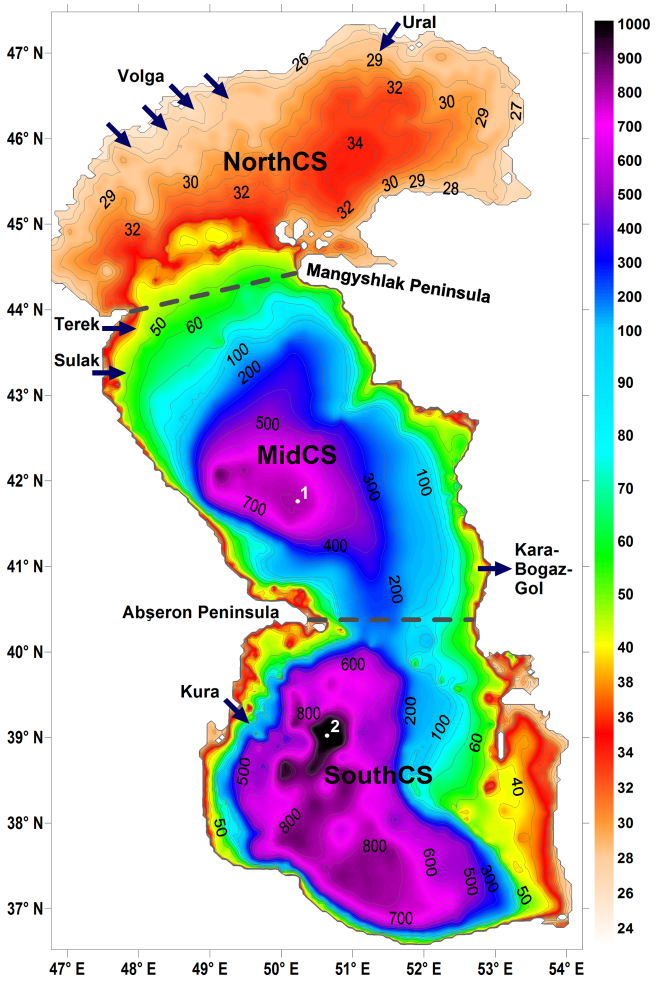

Figure 1. Caspian Sea bathymetry used in the model (depths relative to mean sea level, in meters). The average sea surface height and model vertical grid origin are 28 m. Dashed lines indicate conventional separation of the sea into three basins: northern (NorthCS), middle (MidCS) and southern Caspian (SouthCS). Arrows designate water inflows due to rivers accounted for in the model and the seawater outflow into the Kara-Bogaz-Gol Bay. Numbers 1 and 2 indicate locations of the deepwater stations from Tuzhilkin and Kosarev (2004), for which reference observational T and S data will be given.

3×10^{-4}) $m^2\,s^{-1}$ for diffusivity and thermal conductivity. The model time step is 5 min.

2.2 External forcing

Monthly mean river runoff data were used to prescribe the discharge of the Volga, Ural, Kura, Terek and Sulak rivers. The outflow into the Kara-Bogaz-Gol Bay was set using annual mean data. Atmospheric forcing was prescribed using the ECMWF ERA-40 atmospheric reanalysis dataset (Kallberg et al., 2004), chosen for several reasons. First, the data cover an extended period (from 1957 to 2002) comprising one of the most vivid episodes of global climate change – the climatic regime shift of 1978. This allows for an investigation of the Caspian Sea response to such global events. The other advantage of the ERA-40 reanalysis is its relatively high spatial resolution (1.125°), which is still rather coarse for the Caspian Sea with dimensions 8° × 11°, but it is sufficient to resolve the main features of atmospheric circulation in the region, as has been shown by Ibrayev et al. (2010). The ERA-40 temporal resolution of 6 h allows for the simulation of the diurnal air–sea interaction cycle and the synoptic variability mode. As is the case for any global reanalysis product, ERA-40 has errors specific to a particular region of the planet (Berg et al., 2012; Cattiaux et al., 2013). Therefore, we have partially corrected the ERA-40 wind and precipitation fields for better consistency with the available climatology atlases of the Caspian region (Panin, 1987; Terziev et al., 1992): wind speed was increased by 15 %, and precipitation was decreased by 30 %. The performed corrections as well as the model sensitivity to them are considered in detail in Dyakonov and Ibrayev (2018). The prescribed atmospheric parameters, together with the parameters of the sea surface obtained in the model, are used to compute air–sea fluxes based on the approach of Launiainen and Vihma (1990): evaporation, sensible and latent heat fluxes, and the momentum flux. Precipitation and radiative heat fluxes are taken directly from ERA-40. The fluxes are dynamically amended due to sea ice cover and simulated in the submodel of sea ice thermodynamics, which is described in Schrum and Backhaus (1999).

2.3 Initial conditions and model spin-up

The model was initialized with the climatic mean 3-D fields of temperature and salinity for January (Kosarev and Tuzhilkin, 1995). These fields have been considerably smoothed and averaged over an extended period of time and therefore lack realistic cross-shore gradients and many other details, particularly in shallow regions. While the distribution of temperature in such areas adjusts rather quickly due to atmospheric impact, the salinity field is a lot more passive and requires an additional spin-up model run: the model is run for 5 years with a relaxation of sea surface salinity (SSS) in the southern Caspian basin. This is necessary to avoid excessive growth of salinity in the upper layer of the basin until a freshwater anomaly, associated mainly with the Volga River's runoff, appears along the western coast of the middle Caspian. It is this anomaly that supplies relatively fresh water to the south in an amount sufficient to compensate for intense evaporation. After 5 years a realistic salinity distribution in the middle Caspian is achieved, and the SSS relaxation in the southern Caspian is no longer required to balance the salt budget of this basin. The resultant salinity field is then used as the initial condition for the main model run, as discussed in the following sections.

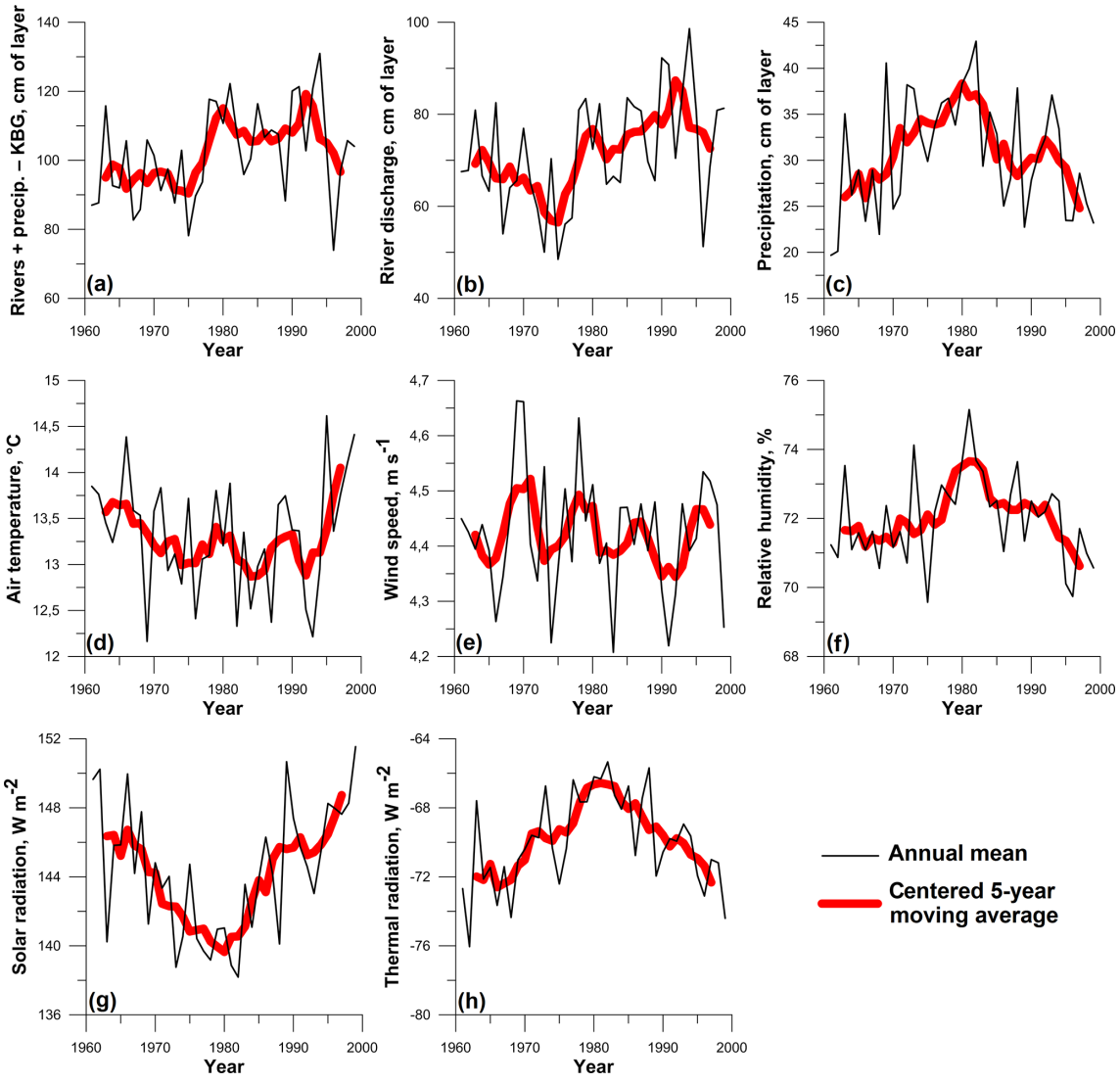

Figure 2. Long-term variability of the forcing components: **(a)** sum of riverine water input and precipitation with the deduction of the outward flux into the Kara-Bogaz-Gol Bay; **(b)** riverine water input alone; **(c)** precipitation; **(d)** air temperature (°C); **(e)** wind speed module ($m\,s^{-1}$); **(f)** relative humidity (%); **(g)** surface solar radiation ($W\,m^{-2}$); **(h)** surface thermal radiation ($W\,m^{-2}$). All atmospheric parameters and fluxes were averaged over the sea area; water fluxes **(a, b, c)** are given in terms of the corresponding sea level increment.

3 External forcing variability

Figure 2 shows the evolution of external forcing components for the period considered. The Caspian Sea water budget is a sum of river discharge ($\sim 300\,km^3\,yr^{-1}$) and precipitation ($\sim 100\,km^3\,yr^{-1}$) approximately balanced by evaporation ($\sim 400\,km^3\,yr^{-1}$) and the outflow into the Kara-Bogaz-Gol Bay ($\sim 30\,km^3\,yr^{-1}$) (Terziev et al., 1992). The underground water contribution is thought to be insignificant ($\sim 4\,km^3\,yr^{-1}$) (Zektser et al., 1984). Evaporation is the only component that cannot be directly measured, and therefore it is computed by the model based on air and sea surface parameters. The evolutions of the net input of the other three water budget components, as well as river discharge and precipitation, are separately presented in Fig. 2a, b and c, respectively. In the late 1970s one can note a sharp rise (~ 20 %) in the net water input, which was a consequence of the climatic regime shift mentioned earlier. The shift was also associated with an increase in air humidity in the Caspian region, followed by a trend change in the evolution of radiative fluxes: both solar and thermal radiation (absolute value) intensities imply warming after 1980. We will refrain from discussing the reasons and mechanisms of such abrupt variations and merely ascertain the fact that the data used to prescribe the external forcing in the model contain the signal associated with the climatic shift of 1978. Notably, there is no significant long-term change in the average air temperature and wind speed module present in the data (Fig. 2d and e).

4 Surface circulation

We start the discussion of the model results with a brief review of surface circulation patterns. This will help to shed some light on further results, as it is the circulation in the upper active layer that mostly determines physical processes occurring in the entire water column. Figure 3 shows monthly mean sea surface currents (SSCs) in January and July, averaged over 1961–1977 (before the regime shift of 1978) and 1978–2001 (after the shift). This division allows for an assessment of how the climatic shift influenced the SSC field. The July pattern was altered insignificantly, so only the plot for the first period is presented. Winter circulation, in contrast, was altered rather noticeably but only in the MidCS basin where the direction of the open sea main flow changed by 45° counterclockwise. We provide these fields only for reference and will not further investigate their variability, as the impact of the climate shift on the SSC is beyond the scope of the present study.

Typical distributions of sea surface salinity (SSS) and temperature (SST) are shown in Fig. 4. Unlike the currents in Fig. 3, these are instantaneous fields, though they clearly correlate with many SSC features. Figure 4a vividly demonstrates the differences in the thermal regime of the three Caspian basins in late winter: while SST in NorthCS is around zero (the basin is covered by an ice sheet), SouthCS waters are much warmer (up to 11 °C). The MidCS basin is subject to intrusions from both the north (cold elongated current propagating along the western shore) and south (warm anomaly in the open sea). The most distinctive feature in the SST field during summer is a cold anomaly in the eastern part of MidCS (Fig. 4b) created by an upwelling, which occurs along the eastern shore due to the northwest wind typical for this region in summer. The same wind accounts for a large freshwater intrusion from NorthCS into MidCS (Fig. 4c), which is formed by a relatively strong jet current near the Mangyshlak Peninsula (see Fig. 3c). Although the existence of this jet is consistent with satellite imagery (Kostianoy et al., 2013), the intensity of the corresponding freshwater transport is evidently overestimated by the model, as these regularly occurring intrusions decrease average SSS in MidCS below that observed by ~ 0.5 psu. This is likely due to excessive numerical viscosity of the tracer advection scheme implemented in the model. Figure 4d shows a reverse situation characterized by an intrusion of relatively salty MidCS waters entering NorthCS and an opposite process occurring along the western MidCS shore. Similar intrusions are noted between the MidCS and SouthCS basins (Fig. 4c, d). Thus, the exchange of water masses with contrasting salinity between Caspian basins plays an important role in the formation of the thermohaline regime of the sea.

5 Model validation

To assess the magnitude of model errors we will compare the evolution of its solution with in situ observations. First let us consider the reconstructed sea surface height (CSSH), which is an integral indicator of the model quality, as it depends on the sea surface temperatures that reflect the thermohaline circulation of the entire sea. Figure 5 compares the observed sea level in the vicinity of Baku (Abşeron Peninsula) with that obtained by the model. Until the sharp decline in 1975 there is a good match of the two curves, which indicates a correct description of seawater balance components. Yet sharp changes in the sea level are not well reproduced in the following period, possibly due to errors in the model and/or inaccuracies in the external forcing data, which led to a considerable discrepancy (up to 35 cm). As a result, the sea surface area is overestimated by the model, and, in turn, so is the net evaporation flux, which is why the model CSSH has a slow downtrend relative to observations and matches them again in 1992. This negative feedback between the Caspian Sea level and its surface area was shown to be significant in earlier work by Dyakonov and Ibrayev (2018). In an auxiliary experiment, accurate water balance was demonstrated when the model was started from 1978 with the correct initial CSSH, which suggests that errors in water budget components occur only in the mid-1970s, i.e., when the first changes in the regime were detected. Overall, the evolution of the Caspian Sea surface height is reconstructed reasonably well, and this fact alone refutes all of the hypotheses relating its rapid rise in 1978–1995 to various earlier speculations in the literature such as changes in the seabed, underground infiltration of the Aral Sea waters into the Caspian, variations in underground riverine discharge and other factors that were not taken into account in the model. Indeed, our results are consistent with the theory of the dominant role of global climate fluctuations in the Caspian Sea level variability on a decadal timescale (Frolov, 2003; Panin and Diansky, 2014). Thus, the sharp growth was caused by the abovementioned climate regime shift of 1978, and the corresponding signal is present in the forcing data we use (Fig. 2b, f).

To analyze deepwater properties we use the long-term measurements of T and S at two particular points located in the central parts of the middle and southern Caspian basins (locations 1 and 2 in Fig. 1) from Tuzhilkin and Kosarev (2004), who studied the evolution of temperature and salinity in deepwater zones of the Caspian Sea in 1956–2000. This interval was divided into four distinct periods: (1) quasi-stationary conditions in 1956–1967, (2) harsh winters and low river influx in 1968–1977, (3) increased river influx in 1978–1995, and (4) regime saturation in 1995–2000. Unfortunately, we do not have the source data available, so only the mean T and S values for these four periods will be used in each location. Figures 6 and 7 compare these averaged values at 100 m of depth to those obtained by the model. Overall, one can note a correlation of the reconstructed evolution

Figure 3. Model monthly mean surface currents in January **(a, b)** and July **(c)** averaged over 1961–1977 **(a, c)** and 1978–2001 **(b)**.

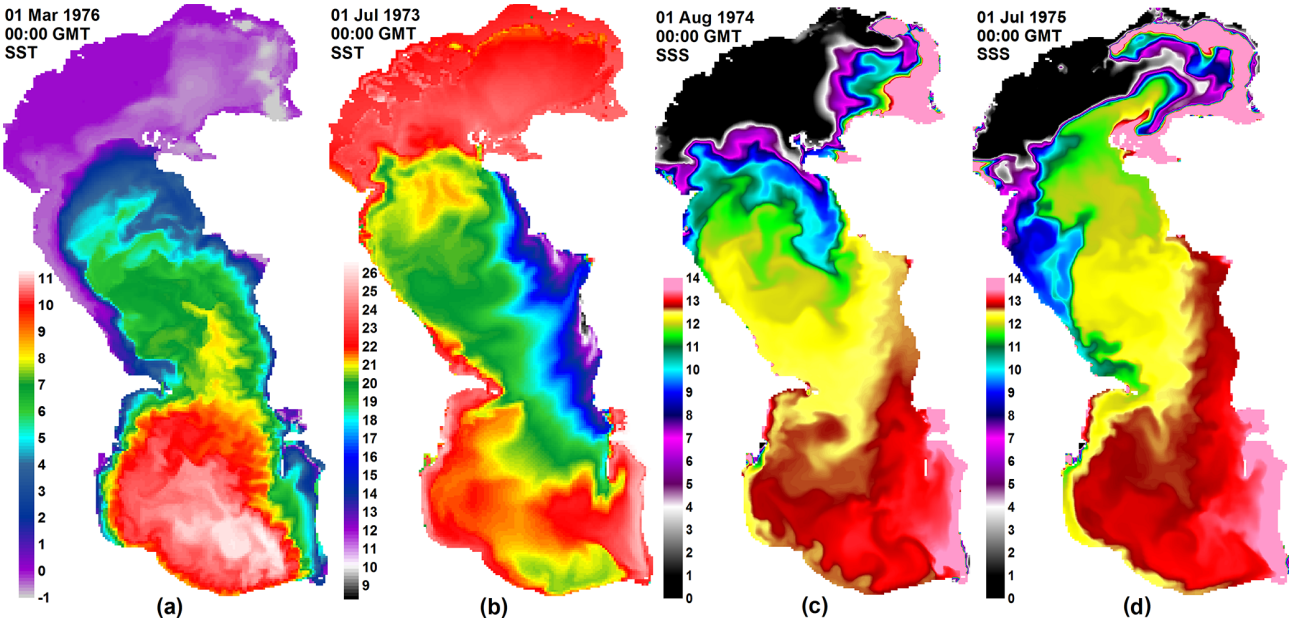

Figure 4. Model instantaneous sea surface temperature (SST) and salinity (SSS): **(a)** SST (°C) on 1 March 1976; **(b)** SST (°C) on 1 July 1973; **(c)** SSS (psu) on 1 August 1974; **(d)** SSS (psu) on 1 July 1975.

with observations, more so in SouthCS than in MidCS. The significant discrepancy in salinity at location 1 is caused by the aforementioned SSS error in MidCS. As a result, salinity stratification of the upper active layer is overestimated in this basin, which obstructs the intense deep convection responsible for the observed increase in salinity at 100 m in 1968–1977 (Fig. 6) caused by the harsh winter conditions of the period. In SouthCS (location 2) model salinity is much closer to observations with the exception of the first period, apparently due to inadequate initial conditions corresponding to the climate mean rather than instantaneous values of 1961. However, in 3 years model salinity reaches values close to the mean observed ones. Systematic overestimation of temperature by 0.5–1.5 °C at both locations reflects errors in the

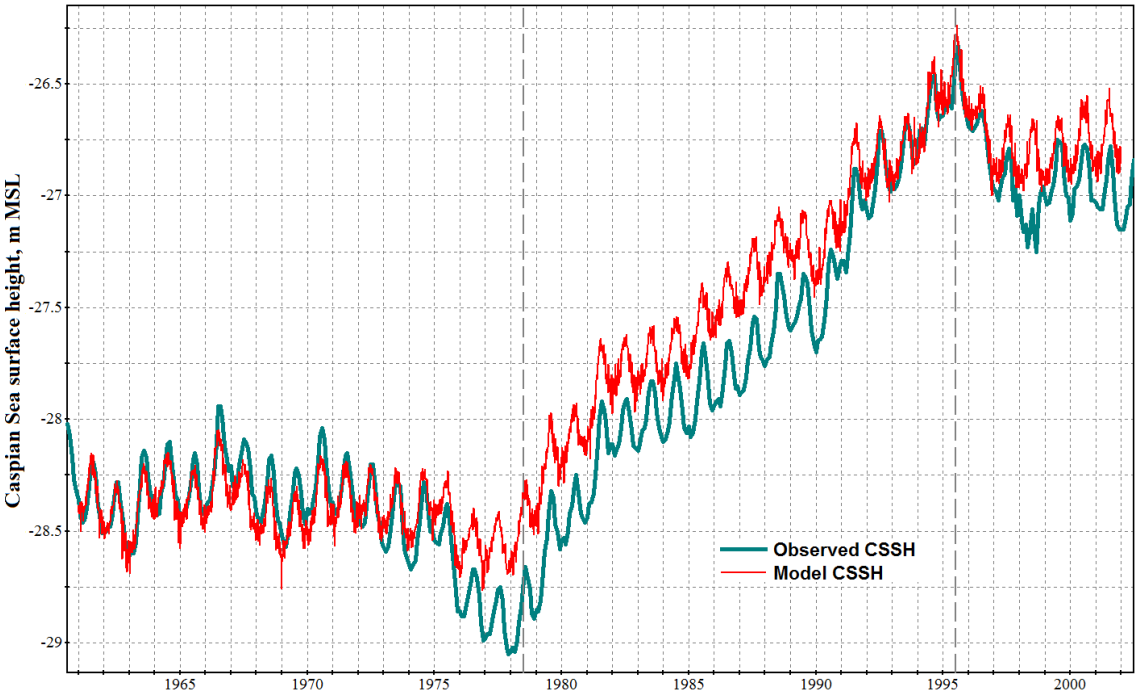

Figure 5. Caspian Sea surface height (CSSH) in the vicinity of Baku: observations and model reconstruction (in meters relative to mean sea level; MSL).

description of vertical mixing, including insufficient convection intensity, and can be considered the model error.

6 Long-term trends of thermohaline properties

6.1 Northern Caspian

The northern Caspian is a very shallow estuary of the Volga and Ural rivers, and the circulation of its waters is strongly influenced by their discharge and wind. Due to the shallow depth (4–5 m in most of its area) the water column is almost always well mixed throughout the year, allowing us to analyze surface properties only. Figure 8 shows the evolution of sea surface salinity (SSS) in all three basins. The amplitude of the SSS annual oscillations increases northward, which is a direct consequence of the riverine runoff distribution in space. As one can see from Fig. 8, SSS in the northern basin fluctuates around 8 psu until the climate regime shift of 1978 and then reaches a new quasi-equilibrium state with an annual mean value slightly below 7 psu. The time required for this transition period is rather small and amounts to 3–4 years. After 1980 the SSS trend stabilizes, but an additional drop down to 6 psu occurs in the 1990s. In the other two Caspian basins SSS trends are similar, but their rates are smaller by an order of magnitude. Overall, SSS evolution in the entire sea correlates with river discharge and air humidity, and the results presented here are consistent with the observations (Tuzhilkin et al., 2011).

Notably, the reconstructed evolution of the NorthCS salinity field is rather sensitive to model design, particularly to the bottom drag parameterization. An important feature of this basin is that it serves as a transit zone for fresh riverine waters, moving into the MidCS and SouthCS basins to be evaporated there. This leads to a continuous loss of the net mass of salt in the northern basin, which can be compensated for only by recurrent intrusions of the MidCS saline waters induced by wind, as shown in Fig. 4d. However, such intrusions are usually brief, so the amount of salt that enters and remains in the northern basin greatly depends on the bottom drag resistance to the currents transporting it. Use of a bottom drag parameterization that is too viscous in our prior experiments caused a gradual decline of mean NorthCS salinity down to zero within a decade. Therefore, a new parameterization scheme that is more adequate for such shallow regions has been devised, which allowed us to stabilize the salinity evolution here at a level close to that observed. Nonetheless, salinity distribution in NorthCS is still somewhat inaccurate compared to observations: the freshwater tongue associated with the Volga River extends southward too far, often shifting the salinity gradient maximum close to MidCS waters (see Fig. 4c). In these conditions, wind drives freshwater masses into the MidCS basin, decreasing its surface salinity down to $\sim$ 12 psu on average (Fig. 8), which is about 0.5–0.7 psu lower than observed.

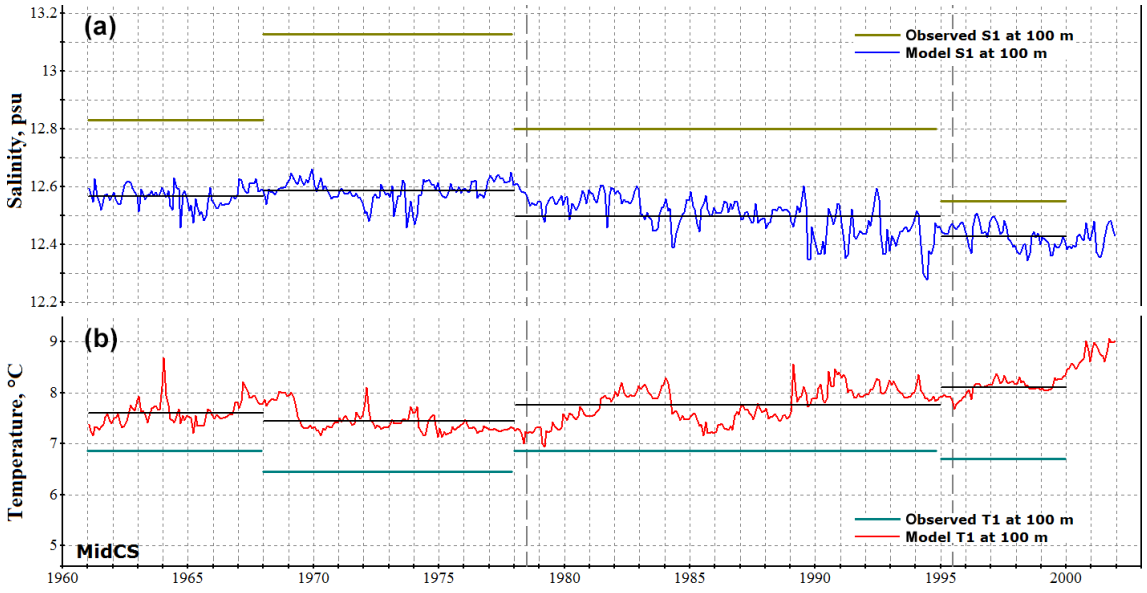

Figure 6. Salinity **(a)** and temperature **(b)** at 100 m of depth at location 1 (MidCS; see Fig. 1) obtained in the model and those observed. The observational data are plotted as a mean value that is constant for four different periods. Mean model values for the corresponding periods are shown in thin black lines.

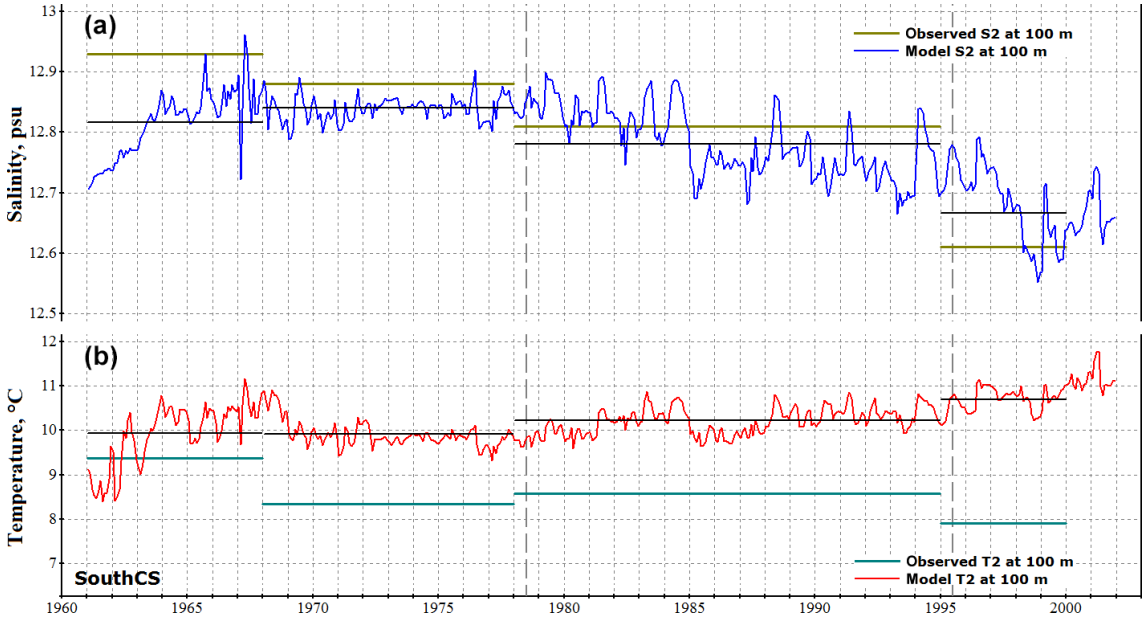

Figure 7. Same as Fig. 6 for location 2 (SouthCS; see Fig. 1).

6.2 Middle Caspian

The middle and southern Caspian basins have maximum depths of 800 and 1000 m, respectively, so vertical mixing processes play a much greater role in thermohaline circulation here than in the north. In MidCS autumn–winter convection is thought to create a mixed layer of 200 m depth and to mix the entire water column during the coldest winters, e.g., in the winter of 1969 (Terziev et al., 1992). However, more recent papers (Tuzhilkin and Goncharov, 2008; Tuzhilkin et al., 2011) suggest that throughout the period considered, convective mixing occurred only in the upper 100 m layer and did not reach the Caspian abyssal waters, even in the most severe winters. Our results support these conclusions: in the numerical reconstruction the average depth of winter convection in the deep parts of the MidCS basin is about 80 m. The abovementioned 0.5–0.7 psu underestimation of MidCS surface salinity significantly decreases convection intensity, but

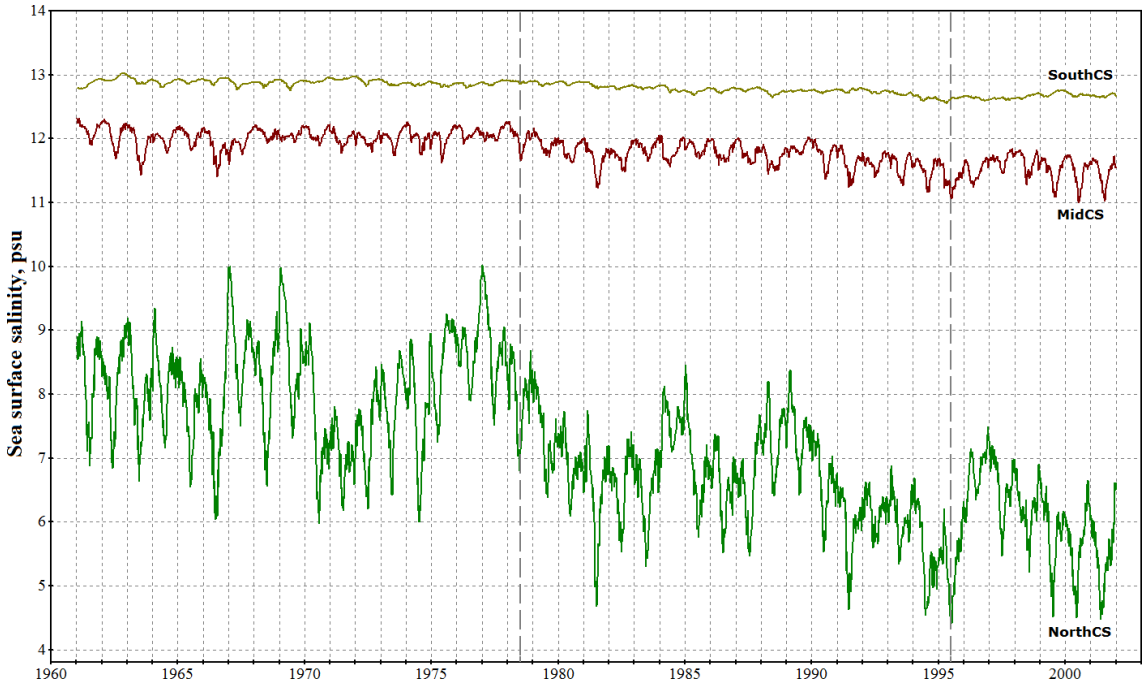

Figure 8. Evolution of sea surface salinity (SSS) averaged over three Caspian basins (psu).

auxiliary sensitivity experiments have shown that convection depth does not exceed 110–120 m, even when this error in the SSS field is artificially compensated for.

Figures 9, 10 and 11 show the reconstructed evolution of salinity, temperature and density at different depths in the MidCS basin. At a depth of 250 m the effects of convective mixing are noted only in the coldest winters and are absent at 500 m and below (Fig. 10). In the active layer (upper 100–150 m) the thermohaline properties exhibit a clear seasonal cycle and have no long-term trend until 1978, which indicates a quasi-stationary circulation regime. After the climate shift of 1978 the upper-layer salinity begins a gradual decline (Fig. 9) associated with the intensification of river discharge and an increase in air humidity in the Caspian region. These downtrends cease only after the next climatic shift in the mid-1990s, when a new quasi-stationary sea circulation regime is achieved. Because the freshening signal, associated with the first shift, originates at the surface, the rate of the salinity downtrend decreases with depth, which strengthens sea stratification and diminishes the convection-driven ventilation of deep waters. These results are qualitatively consistent with observations (Tuzhilkin and Kosarev, 2004; Tuzhilkin et al., 2011). The weakening of convection also accounts for the reduction of winter SST, noted after the shift of 1978 in MidCS, and for the upward trend in subsurface temperatures (Fig. 10), as was suggested in Tuzhilkin et al. (2011).

At greater depths (500 m and deeper) the influence of changes in external conditions becomes almost indistinguishable from the accumulating model errors that account for a slow downtrend (~ 0.1 psu every 40 years) in the average salinity and an uptrend (~ 1 °C every 40 years) in the average temperature. These trends are caused by advective and diffusive mixing and are inevitable in the presence of small but nonzero T and S vertical gradients. According to Tuzhilkin and Goncharov (2008), the only process that can counteract it is down-slope cascading – slow sinking of cold saline waters along the slope of the northern and eastern continental shelves. Despite its important role, this process is not fully taken into account by the model, which is why it yields these erroneous slow trends. The reason is that at depths greater than 30 m the model uses a z coordinate grid, and bottom slope is represented as a set of horizontal stairs obstructing cascading process. To overcome this z coordinate deficiency a parameterization of cascading should be implemented in the model. In the active layer, in contrast, the model errors do not conceal the actual variability of water properties: the long-term trends alternate with quasi-stationary circulation regimes in correlation with external forcing variations.

6.3 Southern Caspian

The reconstructed salinity, temperature and density in the SouthCS basin are presented in Figs. 12, 13 and 14. The southern Caspian basin is the most distant one from the Volga River's mouth and has the strongest evaporation throughout most of the year (Panin, 1987); therefore, the salinity field in its active layer is rather sensitive to water exchange with the relatively less salty MidCS basin. In order to attain a circulation regime that would balance the salt budget of SouthCS, a 5-year spin-up model run with SSS relaxation was neces-

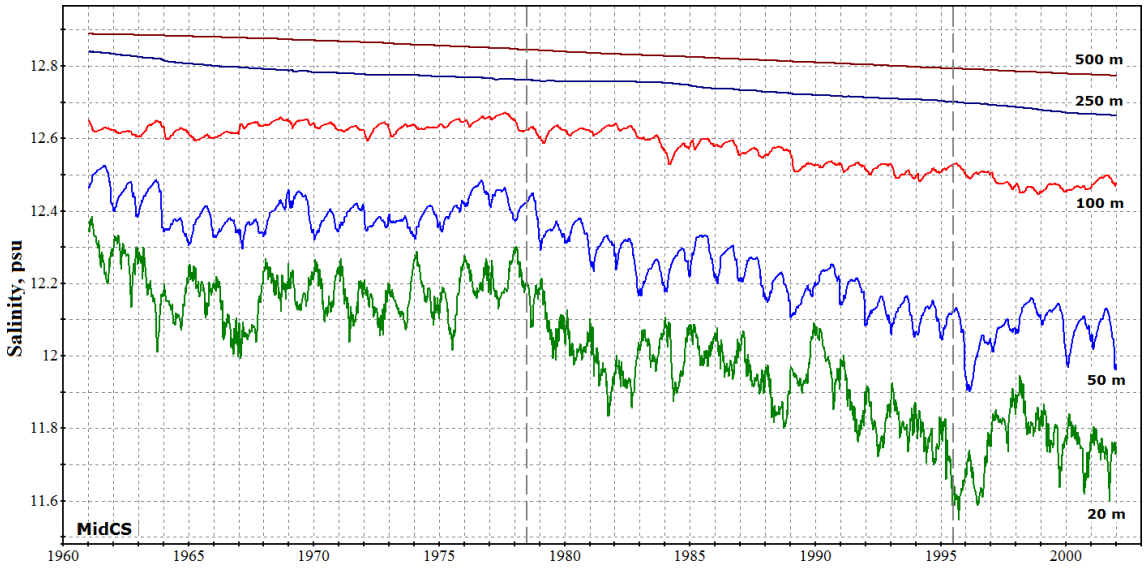

Figure 9. Evolution of salinity (psu) at different depths averaged over the MidCS basin.

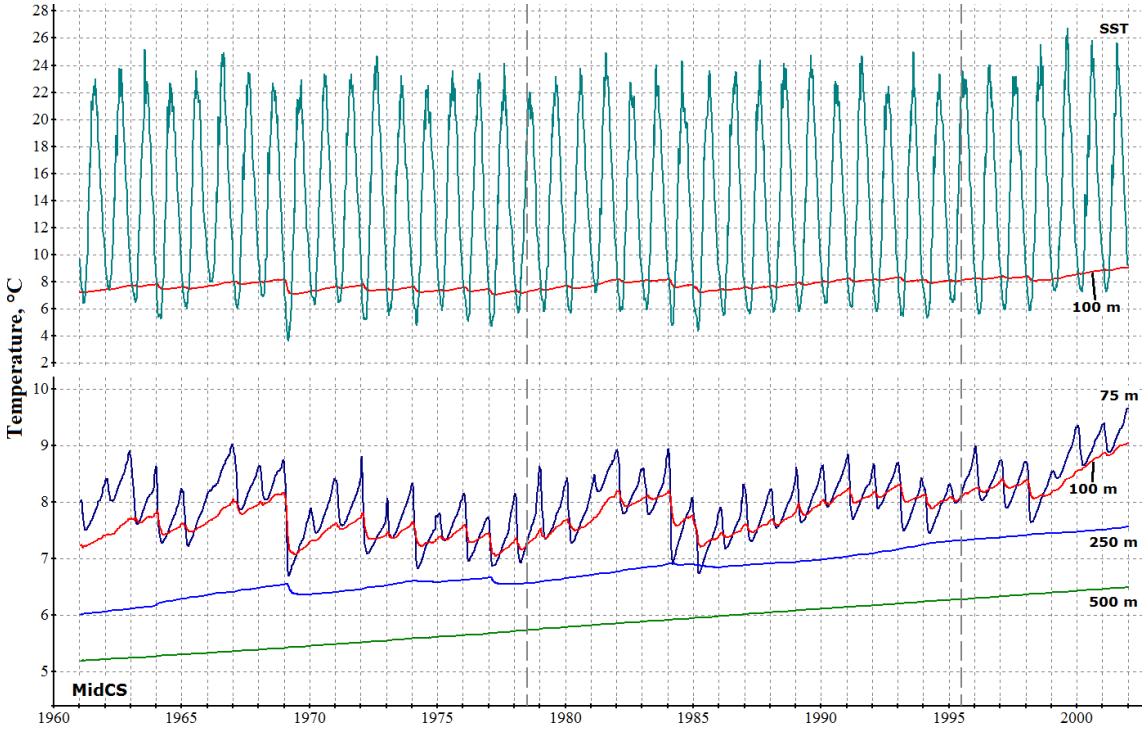

Figure 10. Evolution of temperature at different depths (SST – sea surface temperature) averaged over the MidCS basin (°C).

sary, as we have described in Sect. 2.3. However, after the SSS field had been released, it took three more model years to reach quasi-equilibrium circulation in the upper 100 m sea layer (Figs. 12, 13). During the first 2 years surface salinity grows rapidly, which leads to an intensification of convection-driven mixing in the active layer during the third year of the run with relatively sharp rises in temperature and salinity at the depth of 100 m. By the fourth year of the run (in 1964) a vertically quasi-homogeneous salinity distribution is achieved (Fig. 12), characterized by a slight positive deviation (~ 0.1 psu) in the active layer from the mean climatic values from Kosarev and Tuzhilkin (1995). As a result, the maximum convection depth exceeds that observed by 10–15 m: according to Terziev et al. (1992) convective mixing processes in SouthCS span the upper 70–80 m layer and reach 100 m only in its northern part. In the model recon-

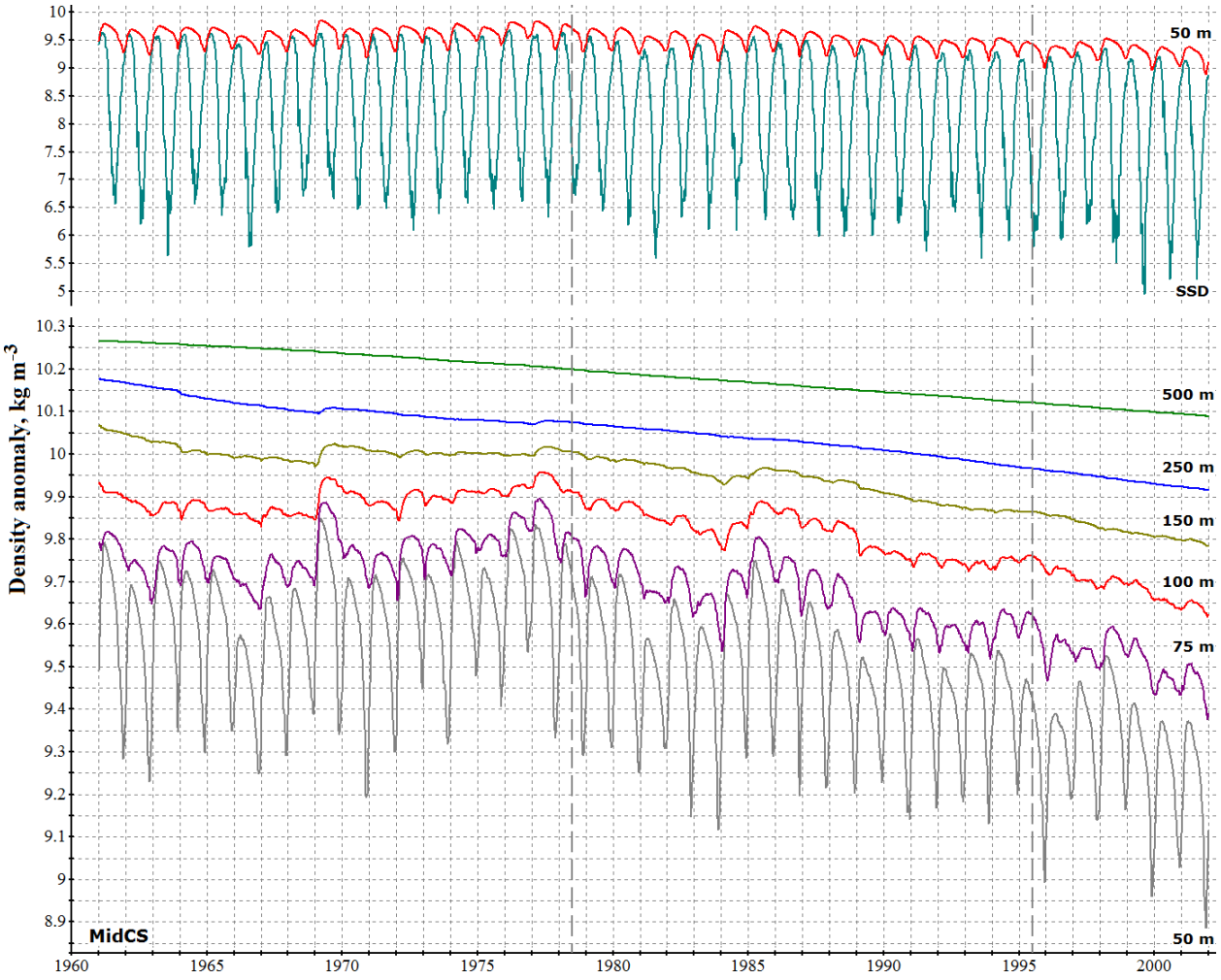

Figure 11. Evolution of a density anomaly (kg m^{-3}) at different depths (SSD – sea surface density) averaged over the MidCS basin.

struction the lower boundary of the convective mixed layer is located at the depth of 80–90 m in the central area of the basin. Thus, average temperatures at 100–150 m are overestimated by 1–2 °C due to overly intense mixing with warmer surface waters during winter.

After the first 4 years of the model run a steady circulation regime is achieved in the upper 100 m layer, which persists until the 1980s. The impact of the climatic shift of 1978 on thermohaline properties in SouthCS is similar to that obtained in MidCS, but it has a 3-year time lag required to adjust MidCS circulation to the forcing variation. In 1981 a transition begins to a new circulation regime characterized by a restoration of stable salinity stratification and an additional increase in temperatures in the lower part of the active layer. Thereby, autumn–winter convection in SouthCS weakens, as can be clearly seen in the evolution of density at 75 m in Fig. 14. Like in the middle Caspian, slow trends in temperature and salinity below 250–300 m in SouthCS are a result of vertical advective and diffusive mixing in the absence of sufficient deepwater ventilation via down-slope cascading from the eastern shelf. At the depth of 250 m the effects of the second climatic shift are still observed, and this is the maximum depth to which a signal of external forcing variability propagates in both the MidCS and SouthCS basins.

7 Summary and conclusions

We have considered a long-term numerical reconstruction of the Caspian Sea thermohaline circulation in 1961–2001. The model reproduced a quasi-stationary regime that lasted until 1978 and, at least qualitatively, the sea response to the global climate shift that occurred in 1976–1978. The influence of surface circulation on the thermohaline regime of the sea has been discussed, and the crucial role of the exchange of waters with contrasting parameters between the three Caspian basins has been demonstrated. A correct reconstruction of the water balance in 1978–1995, i.e., during a period of rapid sea level rise ($\sim$ 2.5 m), confirms that the level rise was associated with the variability of riverine and atmospheric forc-

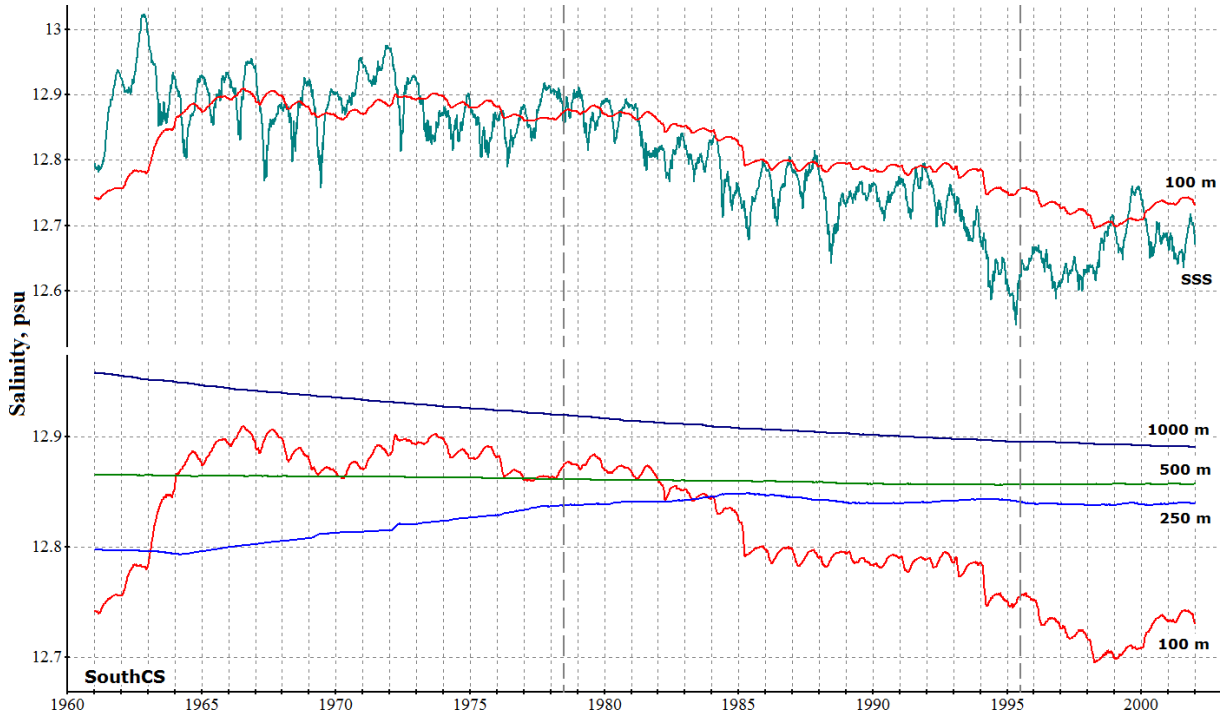

Figure 12. Evolution of salinity (psu) at different depths averaged over the SouthCS basin.

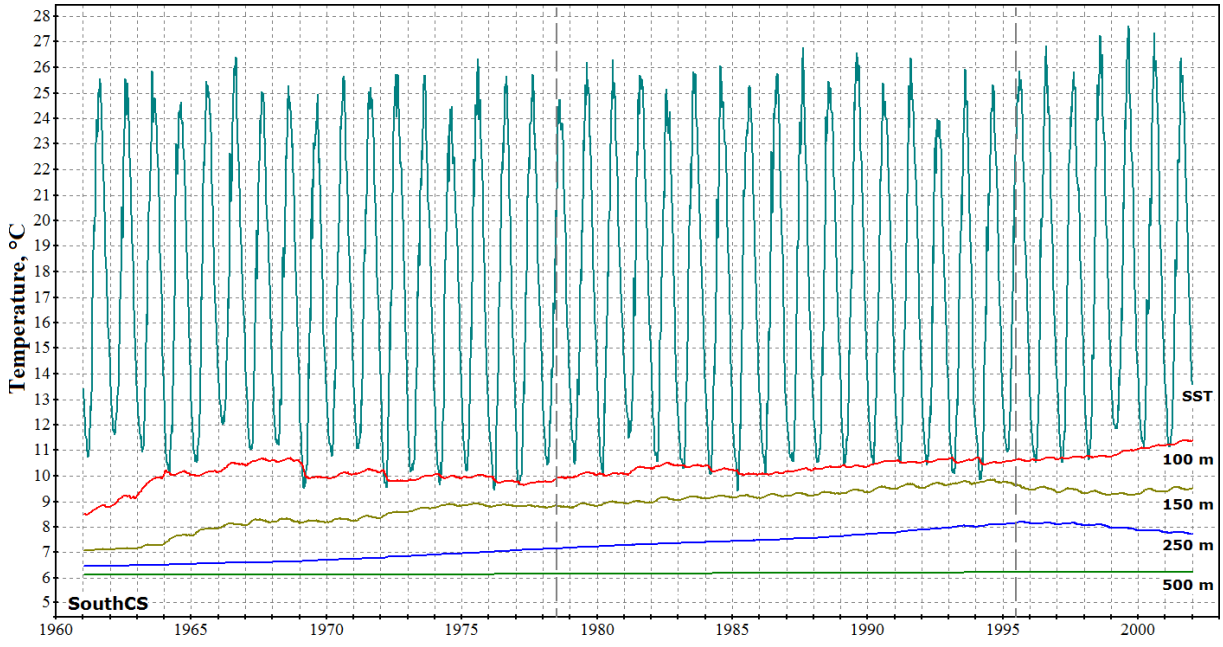

Figure 13. Evolution of temperature at different depths (SST – sea surface temperature) averaged over the SouthCS basin (°C).

ing rather than other factors that are not accounted for by the model. Thus, our results are consistent with the commonly recognized theory relating the Caspian Sea level fluctuations to global climate changes.

During the first 15–17 years of the experiment a quasi-stationary circulation pattern was obtained with a clear seasonal cycle and almost no long-term trends in the evolution of temperature and salinity in the active layer. Due to model errors in reproducing the surface salinity field, the depth of winter convection in the middle Caspian is about half of that estimated in Terziev et al. (1992), although it is in better agreement with the results of more recent studies

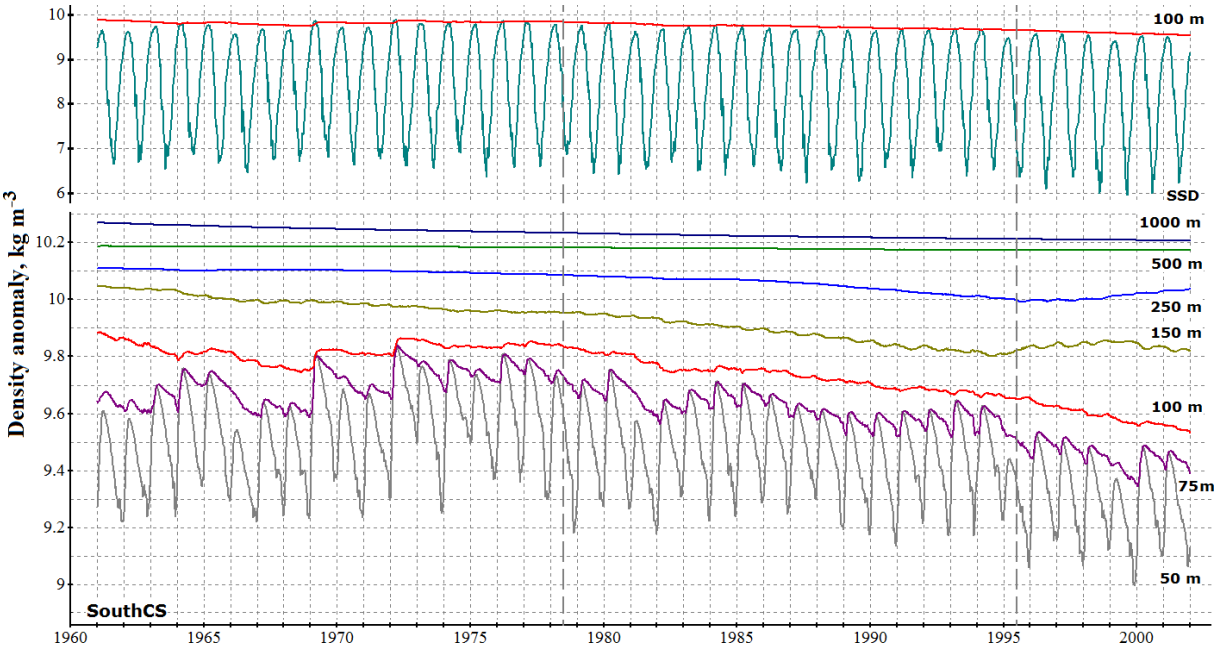

Figure 14. Evolution of a density anomaly (kg m^{-3}) at different depths (SSD – sea surface density) averaged over the SouthCS basin.

(Tuzhilkin and Goncharov, 2008; Tuzhilkin et al., 2011). At greater depths, below the active layer, slow trends in the evolution of thermohaline properties were obtained as a result of the insufficient ventilation of these waters. The reason is that the model does not fully take into account down-slope cascading processes because of the z coordinate. The error accumulation rate amounts to $\sim 1\,^{\circ}$C every 40 years for temperature and ~ 0.1 psu every 40 years for salinity. At intermediate depths (200–300 m) both these trends and the effects of external forcing variability are noted, while below 250–300 m the latter are absent.

After 1978 the non-trend circulation mode was replaced by a transition to a new circulation regime due to a shift that occurred in the global climate. This transition was associated with downtrends in the salinity field, which led to the strengthening of density stratification in the upper sea layers and weakening of autumn–winter convection. As a result of an increased isolation from surface waters during winter, the temperature at 100–200 m showed an uptrend. The surface salinity in the northern and middle Caspian responded to the increased river discharge almost simultaneously, while the corresponding trend in the southern Caspian SSS occurred with a 3-year time lag, which indicates a much greater interdependence of the middle Caspian with the northern basin rather than the southern one. Overall, the reproduced sea response to the climatic shift of 1978 is discernible despite considerable model errors, and it is consistent with the observational data analysis presented in Tuzhilkin et al. (2011). The next climatic shift of 1995 stabilized the salinity trends, and a new circulation regime was achieved.

When modeling Caspian Sea circulation, the greatest challenge is to keep salinity distribution in the active layer close to that observed. Even slight errors in the salinity field significantly modulate the intensity and depth of convective mixing and consequently alter the thermohaline circulation patterns of the entire sea. Two major factors determine the deviations of salinity: external forcing errors and model quality, particularly the description of interbasin water mass exchange, as the three Caspian basins have different salinity regimes. The correct simulation of deepwater properties requires taking into account down-slope cascading, which is an important mechanism of ventilation and renewal of the abyssal Caspian waters. However, despite all of its errors and simplifications, the model qualitatively reproduced the evolution of the Caspian Sea thermohaline circulation and its response to external forcing variations.

Data availability. The air forcing was prescribed using data from the ECMWF ERA-40 reanalysis available at https://apps.ecmwf.int/datasets/data/era40-daily/levtype=sfc/ (ECMWF, 2009). The gridded ETOPO1 bathymetry is provided by NOAA's National Centers for Environmental Information available at https://www.ngdc.noaa.gov/mgg/global/global.html (NOAA/NCEI, 2013). The Caspian Sea model source code currently has no software license and therefore cannot be made publicly available.

Author contributions. The research was carried out by GD under the supervision of RI.

Competing interests. The authors declare that they have no conflict of interest.

Acknowledgements. The research was carried out using equipment from the shared research facilities and HPC computing resources at Lomonosov Moscow State University (Sadovnichy et al., 2013) and Joint Supercomputer Center of the Russian Academy of Sciences.

Financial support. The work was carried out at the Northern Water Problems Institute of the Karelian Research Center with the financial support of Russian Science Foundation grant no. 14-17-00740.

Review statement. This paper was edited by Markus Meier and reviewed by Emin Özsoy and two anonymous referees.

References

Amante, C. and Eakins, B. W.: ETOPO1 1 Arc-Minute Global Relief Model: Procedures, Data Sources and Analysis, NOAA Technical Memorandum NESDIS, NGDC-24, National Geophysical Data Center, NOAA, 25 pp., https://doi.org/10.7289/V5C8276M, 2009.

Arkhipkin, V. S., Bondarenko, A. L., Vedev, D. L., and Kosarev, A. N.: Peculiarities of water circulation at eastern coast of the Middle Caspian Sea, Vodnye Resursy, 6, 36–43, 1992 (in Russian).

Arpe, K., Bengtsson, L., Golitsyn, G. S., Mokhov, I. I., Semenov, V. A., and Sporyshev, P. V.: Analysis and modeling of the hydrological regime variations in the Caspian Sea basin, Dokl. Earth Sci., 366, 552–556, ISSN 1028-334X (print), 1531-8354 (electronic version), 1999.

Berg, P., Feldmann, H., and Panitz, H. J.: Bias correction of high resolution regional climate model data, J. Hydrol., 448–449, 80–92, https://doi.org/10.1016/j.jhydrol.2012.04.026, 2012.

Cattiaux, J., Douville, H., and Peings, Y.: European temperatures in CMIP5: origins of present-day biases and future uncertainties, Clim. Dynam., 41, 2889–2907, https://doi.org/10.1007/s00382-013-1731-y, 2013.

Diansky, N. A., Fomin, V. V., Vyruchalkina, T. Y., and Gusev, A. V.: Reproduction of the Caspian Sea circulation with calculation of the atmospheric forcing using the WRF model, Trudy KarNC, 5, 21–34, https://doi.org/10.17076/lim310, 2016 (in Russian).

Dyakonov, G. S. and Ibrayev, R. A.: Description of coastline variations in an ocean general circulation model, Izv. Atmos. Ocean. Phys., 52, 535–541, https://doi.org/10.1134/S0001433816050054, 2016.

Dyakonov, G. S. and Ibrayev, R. A.: Reproduction of interannual variability of the Caspian Sea level in a high-resolution hydrodynamic model, Oceanology, 58, 8–18, https://doi.org/10.1134/S0001437018010046, 2018.

ECMWF: ERA-40 reanalysis, available at: https://apps.ecmwf.int/datasets/data/era40-daily/levtype=sfc/, last access: 28 July 2009.

Frolov, A. V.: Modeling of the Long-Term Level Fluctuations of the Caspian Sea: Theory and Use, GEOS, Moscow, ISBN 5-89118-298-X, 2003 (in Russian).

Griffies, S. M. and Hallberg, R. W.: Biharmonic friction with a Smagorinsky-like viscosity for use in large-scale eddy-permitting ocean models, Mon. Weather Rev., 128, 2935–2946, https://doi.org/10.1088/1742-6596/16/1/048, 2000.

Gündüz, M. and Özsoy, E.: Modelling seasonal circulation and thermohaline structure of the Caspian Sea, Ocean Sci., 10, 459–471, https://doi.org/10.5194/os-10-459-2014, 2014.

Ibrayev, R. A.: Model of enclosed and semi-enclosed sea hydrodynamics, Russ. J. Numer. Anal. M., 16, 291–304, https://doi.org/10.1515/rnam-2001-0404, 2001.

Ibrayev, R. A.: Mathematical Modeling of Thermodynamics Processes in the Caspian Sea, GEOS, Moscow, ISBN 978-5-89118-418-3, 2008 (in Russian).

Ibrayev, R. A. and Dyakonov, G. S.: Modeling of ocean dynamics with large variations in sea level, Izv. Atmos. Ocean. Phys., 52, 455–466, https://doi.org/10.1134/S000143381604006X, 2016.

Ibrayev, R. A., Sarkisyan, A. S., and Trukhchev, D. I.: Seasonal variability of the circulation of the Caspian Sea reconstructed from mean multi-year hydrological data, Izv. Atmos. Ocean. Phys., 37, 96–104, 2001.

Ibrayev, R. A., Özsoy, E., Schrum, C., and Sur, H. I.: Seasonal variability of the Caspian Sea three-dimensional circulation, sea level and air-sea interaction, Ocean Sci., 6, 311–329, https://doi.org/10.5194/os-6-311-2010, 2010.

Kallberg, P., Simmons, A., Uppala, S., and Fuentes, M.: ERA-40 Project Report Series No. 17, European Centre for Medium Range Weather Forecasts, Reading, 2004.

Kara, A. B., Wallcraft, A. J., Metzger, E. J., and Gunduz, M.: Impacts of freshwater on the seasonal variations of surface salinity and circulation in the Caspian Sea, Cont. Shelf Res., 30, 1211–1225, https://doi.org/10.1016/j.csr.2010.03.011, 2010.

Kosarev, A. N. and Tuzhilkin, V. S.: Climatic Thermohaline Fields in the Caspian Sea, Sorbis, Moscow, 92 pp., ISBN 5-88403-004-6, 1995 (in Russian).

Kostianoy, A. G., Lebedev, S. A., and Solovyov, D. M.: Satellite Monitoring of the Caspian Sea, Kara-Bogaz-Gol Bay, Sarykamysh and Altyn Asyr Lakes, and Amu Darya River, in: The Turkmen Lake Altyn Asyr and Water Resources in Turkmenistan. The Handbook of Environmental Chemistry, edited by: Zonn, I. and Kostianoy, A., vol. 28, Springer, Berlin, Heidelberg, https://doi.org/10.1007/698_2013_237, 2013.

Launiainen, J. and Vihma, T.: Derivation of turbulent surface fluxes – an iterative flux-profile method allowing arbitrary observing heights, Environ. Softw., 5, 113–124, 1990.

Miller, A. J., Cayan, D. R., Barnett, T. P., Graham, N. E., and Oberhuber, J. M.: The 1976–77 climate shift of the Pacific Ocean, Oceanography, 7, 21–26, 1994.

Munk, W. H. and Anderson, E. R.: Note on the theory of the thermocline, J. Mar. Res., 7, 276–295, 1948.

NOAA/NCEI: ETOPO1 bathymetry, available at: https://www.ngdc.noaa.gov/mgg/global/global.html, last access: 10 February 2013.

Panin, G. N.: Evaporation and Heat Exchange in the Caspian Sea, Nauka, Moscow, 88 pp., 1987 (in Russian).

Panin, G. N. and Diansky, N. A.: On the correlation between oscillations of the Caspian Sea level and the North Atlantic climate, Izv. Atmos. Ocean. Phys., 50, 266–277, https://doi.org/10.7868/S0002351514020084, 2014.

Powell Jr., A. M. and Xu, J.: Abrupt Climate Regime Shifts, Their Potential Forcing and Fisheries Impacts, Atmospheric and Climate Sciences, 1, 33–47, https://doi.org/10.4236/acs.2011.12004, 2011.

Sadovnichy, V., Tikhonravov, A., Voevodin, V., and Opanasenko, V.: "Lomonosov": Supercomputing at Moscow State University, in: Contemporary High Performance Computing: From Petascale toward Exascale, Chapman & Hall/CRC Computational Science, CRC Press, Boca Raton, USA, 283–307, ISBN 9781466568358, 2013.

Schrum, C. and Backhaus, J. O.: Sensitivity of atmosphere-ocean heat exchange and heat content in North Sea and Baltic Sea: a comparative assessment, Tellus A, 51, 526–549, https://doi.org/10.1034/j.1600-0870.1992.00006.x, 1999.

Sweby, P.: High resolution schemes using flux limiters for hyperbolic conservation laws, SIAM J. Numer. Anal., 21, 995–1011, 1984.

Terziev, F. S., Kosarev, A. N., and Kerimov, A. A. (Eds.): Hydrometeorology and Hydrochemistry of the Soviet Seas, Vol. 6: The Caspian Sea, No. 1: Hydrometeorological Conditions, Gidrometeoizdat, St. Petersburg, 1992 (in Russian).

Tuzhilkin, B. S. and Kosarev, A. N.: Long-term variations in the vertical thermohaline structure in deep-water zones of the Caspian Sea, Water Resour., 31, 376–383, https://doi.org/10.1023/B:WARE.0000035677.81204.07, 2004.

Tuzhilkin, V. S. and Goncharov, A. V.: On deep water ventilation in the Caspian Sea, Trudy GOIN, 211, 43–64, ISSN 0371-7119, 2008 (in Russian).

Tuzhilkin, V. S., Kosarev, A. N., Arkhipkin, V. S., and Nikonova, R. E.: Long-term variations of the hydrological regime of the Caspian Sea, Vestnik Moskovskogo Universiteta Geography, 2, 62–71, 2011 (in Russian).

Wooster, W. S. and Zhang, C. I.: Regime shifts in the North Pacific: early indications of the 1976–1977 event, Prog. Oceanogr., 60, 183–200, https://doi.org/10.1016/j.pocean.2004.02.005, 2004.

Zektser, I. S., Dzhamalov, R. G., and Meskheteli, A. V.: Underground Water Balance between Land and Sea, Gidrometeoizdat, Leningrad, 206 pp., 1984 (in Russian).